GEOPHYSICS, VOL. 77, NO. 4 (JULY-AUGUST 2012); P. WB119–WB126, 7 FIGS., 1 TABLE.
10.1190/GEO2011-0378.1

Feasibility of monitoring hydraulic fracturing using time-lapse audio-magnetotellurics

Lanfang He[1], Xiumian Hu[2], Ligui Xu[3], Zhanxiang He[3], and Weili Li[3]

ABSTRACT

Hydraulic fracturing is widely used for initiating and subsequently propagating fractures in reservoir strata by means of a pressurized fluid to release oil and gas or to store industry waste. Downhole or surface microseismic monitoring is commonly used to characterize the hydraulically induced fractures. However, in some cases, downhole microseismic monitoring can be difficult due to the limitation imposed by boreholes. Surface microseismic monitoring often faces difficulties acquiring high signal-to-noise ratio data because of the on-site noise from hydraulic fracturing process. Research and field observations indicate that injecting conductive slurry or water into a strata may generate distinct time-lapse electromagnetic anomalies between pre- and posthydraulic fracturing. These anomalies provide a means for characterizing the hydraulic fracturing using time-lapse electromagnetic methods. We examined the time-lapse variation over an hour, one day, one month, and two years of observed audio-magnetotellurics (AMT) resistivity and the 1D and 3D AMT modeling result of the variation pre- and post-hydraulic fracturing. There is also a successful case history of applying the time-lapse AMT to map hydraulic fractures. Observed data indicate that the variation of AMT resistivity is normally less than 6% apart from the data of the dead band and some noisy data. Modeling results show the variation pre- and posthydraulic fracturing is larger than 30% at the frequency point lower than 100 Hz. The case history indicates that time-lapse magnetotelluric monitoring may form a new way to characterize the hydraulic fracture.

INTRODUCTION

Hydraulic fracturing is one of the basic methods that is commonly used to enhance productivity in hydrocarbon and geothermal reservoirs, or as a tool for disposal of oilfield waste (e.g., Wong and Farmer, 1973; Stow and Haase, 1986; Stanchits et al., 2011). Experiences in unconventional gas development and conventional oil and gas production show that hydraulic fracturing is almost always necessary to make the resource extraction profitable (e.g., Kent and Lee, 2007; Arthur et al., 2008). The research on characterizing hydraulic fractures has mostly focused on surface and downhole microseismic (e.g., Maxwell, 2010, 2011; Song et al., 2010), vertical seismic profiling (e.g., Willis, 2007) and downhole and surface tiltmeter techniques (e.g., Warpinskil et al., 1997; Saleh and Blum, 2005). Microseismic imaging has proven valuable in visualizing the geometry of hydraulic fractures (Maxwell, 2011). In some cases, however, downhole monitoring cannot be conducted due to the limitations imposed by boreholes. During surface microseismic monitoring, is it somewhat difficult to acquire high signal-to-noise ratio data because of the ambient noise from the hydraulic fracturing process. In other cases, microseismic monitoring has proven difficult because of a high level of background microearthquakes. Hydraulic fracturing mapping in these cases calls for other monitoring methods.

Recent research has discovered that fracture of quartz-bearing rocks and other hard piezoelectric materials, such as coal-rock bodies or shale, is associated with radio frequency electromagnetic (EM) emissions (e.g., Nitsan, 1977; Steven et al., 1995; Frid et al., 2003; Frid and Vozoff, 2005; Cuevas et al., 2009; Nie et al., 2009). Recent studies also indicate that the injection of cold water into a

Manuscript received by the Editor 26 October 2011; revised manuscript received 14 March 2012; published online 10 July 2012.
[1]Nanjing University, State Key Laboratory of Mineral Deposits Research, School of Earth Sciences and Engineering, China; China National Petroleum Corporation; BGP, Nonseismic, China. E-mail: mofoo@263.net.
[2]Nanjing University, State Key Laboratory of Mineral Deposits Research, School of Earth Sciences and Engineering, China. E-mail: huxm@nju.edu.cn.
[3]China National Petroleum Corporation; BGP, Non-seismic, China. E-mail: xulg@bgp.com.cn; hezhanxiangbgp@yahoo.com; Liweili@cnpc.com.cn.
© 2012 Society of Exploration Geophysicists. All rights reserved.

hydrocarbon reservoir may generate self-potential anomalies and natural seismicity may induce a seismoelectromagnetic signal as a result of the electrokinetic effect (e.g., Hunt, 2007; Murtaza Gulamali, 2011). Orange et al. (2009) discuss the feasibility of reservoir monitoring using time-lapse marine CSEM with 2D reservoir-depletion modeling; they find there could be a measurable changes in a CSEM response if 10% of a resistive hydrocarbon reservoir is replaced by conductive pore fluids. Wang et al. (1991) use a borehole-to-surface electrical resistivity method to map the resistivity difference before and after a hydraulic fracturing treatment was performed with a conductive fluid. Wilt and Morea (2004) carry out crosshole EM mapping of the resistivity variation before and after hydraulic fracturing; the result indicated that resistivity difference is as high as 38%. Laboratory resistivity measurement shows that, if the injected slurry used in hydraulic fracturing features has a low resistivity, it might directly generate measurable surface resistivity anomalies. All of these studies suggest that the requisite conditions exist for characterizing the hydraulic fracturing using time-lapse electromagnetic methods. The audio-magnetotelluric (AMT) method, which was developed from the conventional magnetotelluric method, has recently seen widespread applications in engineering, groundwater, environmental, petroleum, mining, and geotechnical explorations (e.g., Sheard et al., 2005; Rajib et al., 2010; Chalikakis et al., 2011). AMT has proven to be a method that can detect changes in the electrical resistivity and consequently to be useful for time-lapse monitoring (e.g., Falgas et al., 2006).

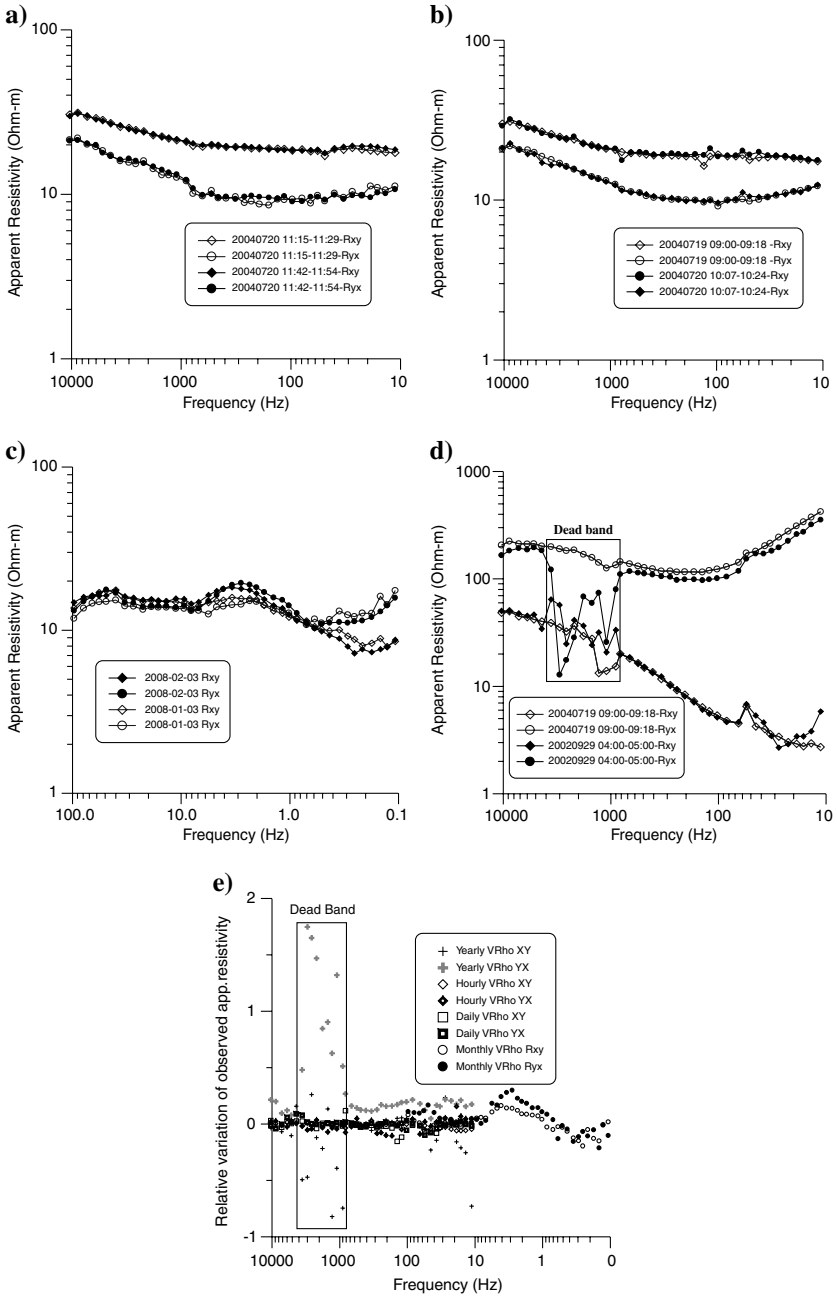

Figure 1. Hourly, daily, monthly, and yearly variation of AMT observed apparent resistivity. (a) The comparison result with a time lapse of one hour, (b) is that of one day, (c) has a time lapse of one month, (d) is a yearly result with a duration of more than two years, and (e) is a scatter diagram of the relative rho variation.

In this paper, we explore hydraulic fracturing monitoring using time-lapse audio-magnetotellurics. The work is based on an AMT monitoring operation at a test area in southwest China. We first discuss the predictions of the time-lapse AMT application; the expected temporal variations of the observed AMT apparent resistivity with and without stimulation. Then we show the laboratory resistivity measurements involving the injected slurry used in hydraulic fracturing, and discuss the 1D and 3D modeling to estimate the observed apparent resistivity variations on the surface before and after hydraulic fracture. Finally, we review the field operations and discuss the result of a case study of using time-lapse AMT monitoring for hydraulic fracture.

NATURAL TIME VARIATION OF AMT APPARENT RESISTIVITIES

AMT data are sensitive to the subsurface resistivity according to the fundamental Tikhonov-Cagniard (T-C) model. The fundamental MT assumption is that the EM field, due to external sources at Earth's surface, behaves as a plane wave. The two horizontal components of the electric field are linearly related to the two horizontal magnetic field components. The proportionality between the E and H fields on the surface depends on the distribution of the electrical resistivity in the subsurface (Eisel and Egbert, 2001). When there is no variation with time in subsurface geoelectrical structures, the observed AMT apparent resistivities should remain constant. In practice, the observed apparent resistivities do change slightly over time. Eisel and Egbert (2001) study the temporal variation of magnetotelluric transfer functions estimated at two MT stations in central California over a period of two years. Their results indicate daily variation from 2% to 5% at periods of 10–1000 s.

Hanekop and Simpson (2006), using data from a control site situated on a stable craton in central Australia to study the stability of MT transfer functions, found apparent-resistivity variations of ~3% (for periods ~100 s over 24–48 h intervals). Chiang et al. (2008) used AMT data from Taiwan's Chelungpu fault, and they have observed a maximum time variation of 43% in apparent resistivity and 18° in phase between 2004 and 2005. These early research results provide us with the expected range of time-lapse AMT responses due to naturally occurring phenomena.

Given that the natural time variation is an important background variation in time-lapse AMT monitoring of oil and gas production, we have also carried out a similar study using field data acquired at two stations located in China, and another station located in Pest, Hungary. Yearly time-lapse data were extracted from measurements at the two projects. Both projects have a duration of 22 months. Monthly time-lapse data were extracted from a reference station in Pest because no monthly repeat observations were performed at any one of the regular stations of that project. The monthly data are in a higher-frequency portion of the MT spectrum. Unlike AMT, the frequency ranges from 0.1 to 97 Hz. The relative apparent resistivity variation is quantified by the following relative change

$$\delta = 1 - \frac{\rho_{a1}}{\rho_{a2}}, \tag{1}$$

where δ is the relative change, and ρ_{a1} and ρ_{a2} are the apparent resistivities at two different times t 1 and t 2.

The results are shown in Figure 1. Figure 1c is the data from Pest. Figure 1a, 1b, and 1d is the data from China. The apparent resistivity curves acquired at different times have a similar shape. The normal variation at all periods is <6% (Figure 1e), except the dead band where noise dominates. The high repeatability indicates that the observed AMT apparent resistivity is generally stationary above the 6% threshold, except in some cases where it is higher because of the natural seismicity. That AMT can be used for time-lapse monitoring. The observed variation with time also sets a lower limit of detectability in time-lapse monitoring. Furthermore, the dead-band AMT frequencies between 1 and 5 kHz, in which the natural energy source has a signal minimum (Garcia and Jones, 2005), should not be used in AMT time-lapse monitoring.

LABORATORY RESISTIVITY MEASUREMENT

To analyze the resistivity variation of the hydraulic fracture injected with slurry composed of water and cement, a test block has been made for laboratory resistivity measurements. The test block is 5 cm in height, 10 cm in length, and 10 cm in width. A polymethyl methacrylate box was used to contain the solidification. A DC resistivity pole-pole array (Figure 2a) was used to measure the wet slurry and a DC Schlumberger array (Figure 2b) was used to test the solidified block. We preferred the Schlumberger array, but were unable to set it up for the wet slurry before solidification. For that reason, the first set of measurements was taken using the pole-pole array. Figure 2c shows the results. The measured resistivity of the test block was <1 ohm-m in the first three days and then increased. The resistivity of the block reached 40 ohm-m after 40 days later, and further increased to 840 ohm-m after 90 days. The resistivity value eventually reached 4900 ohm-m after solidification. The results show that the injected slurry appears as a low resistivity fluid at the beginning of the hydraulic fracture process, but turns into a highly resistive solid after several months. Dehydration of the slurry would have contributed to the resistivity changes while it transitioned from watery slurry to dry cement. The mineralized water dominates the resistivity of the conductive wet block, whereas the solid matrix of the cement dominates that of the resistant dry block. These laboratory measurements provide important information to interpret AMT monitoring data in operations. Any previous injection would remain as a resistive anomaly, but the newly injected slurry would reduce the observed apparent resistivities on the surface shortly after the hydraulic fracture. This is possible in tight shale, because groundwater does not come into contact with the slurry. The water in the slurry returns to the surface during the

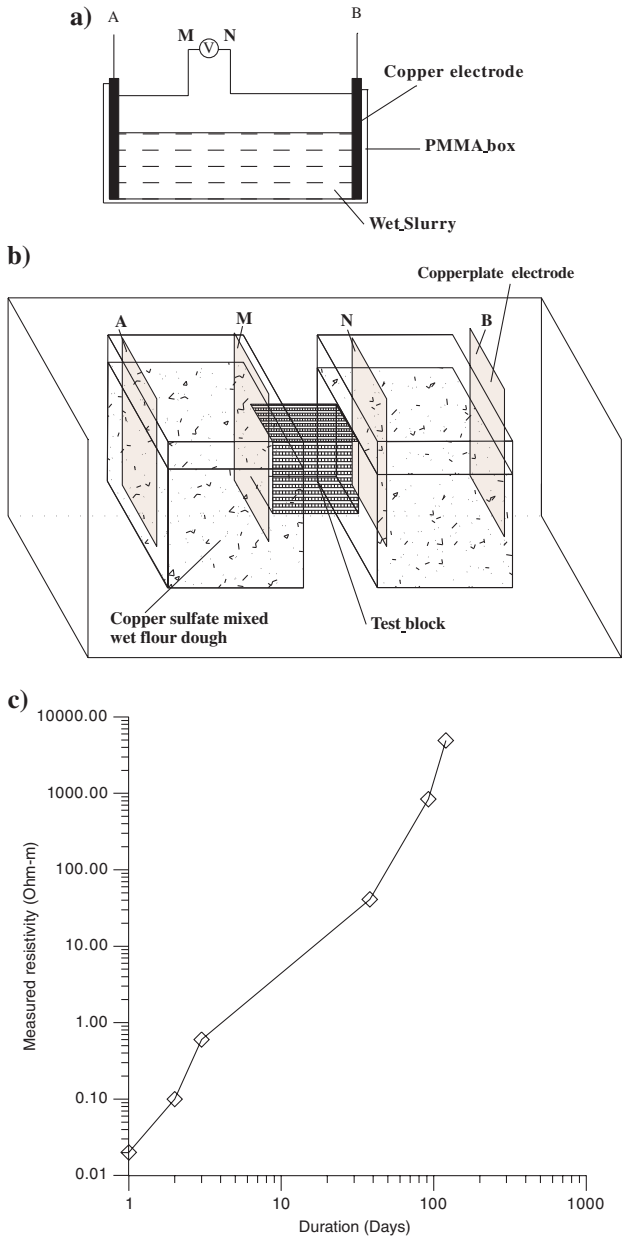

Figure 2. Laboratory resistivity measurement of the test block. (a and b) The sketch map for measuring the resistivity of wet and solidified slurry, and (c) is the measured result.

Table 1. Parameters of 1D and 3D models.

No.	Depth (m)	Thickness (m)	Mod 1D ρ (Ohm-m)	Mod 3D ρ (Ohm-m)
1	10	10	100	100
2	100	90	100	100
3	240	140	250	250
4	360	120	250	250
5	362	2	2000/0.5	2000/0.5
6	392	30	2000	2000
7	432	40	250	250
8	472	40	250	250
9	552	80	250	250
10			500	500

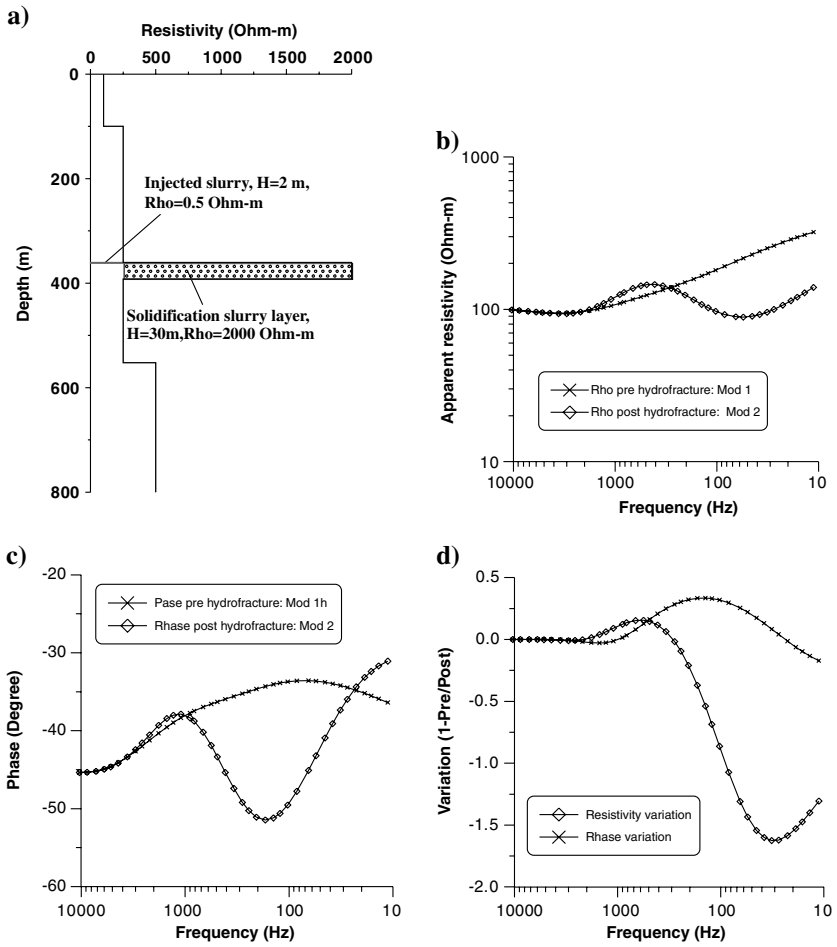

Figure 3. The 1D model and the modeling result. (a) The 1D model. The injected layer is buried about 360 m, the thickness of the solidification slurry layer is 30 m with a resistivity of 2000 ohm-m, the injected slurry is 2 m with 2000 ohm-m prehydrofracture (model-1) and 0.5 ohm-m posthydrofracture (model-2). (b) The apparent resistivity comparison of modeling result of model-1 and model-2. (c) The phase comparison result, and (d) the variation pre- and posthydraulic fracture.

slurry solidification after a pressure relief valve is opened. We have carried out numerical modeling based on this conceptual model and the associated resistivity measurements in the laboratory.

NUMERICAL MODELING

We have performed 1D and 3D modeling to examine the expected surface apparent resistivity difference before and after hydraulic fracturing. The 1D geoelectrical model we use is based on the assumption that the previous hydraulic fracturing has been carried out and the slurry is in the state of consolidation with as high a resistivity as 2000 ohm-m and a thickness of 30 m. The injected slurry is assumed to have a resistivity of 0.5 ohm-m and a thickness of 2 m. The resistivity depth-profile of the host rock is listed in Table 1. The depth to the top of the slurry is set at 360 m. We have constructed four 3D models. Model-1 simulates the prehydrofracturing case in which no conductive layer is injected. Model-2 has an injected conductive zone of 300 × 300 × 2 m with a resistivity of 0.5 ohm-m. Model-3 increases the thickness of the 0.5 ohm-m conductive zone to 18 m, whereas model-4 enlarges the width of the 2 m thick slurry zone to 900 m in both horizontal directions. The finite difference algorithm of Mackie et al., (1993, 1994) was used for 3D EM modeling. Figure 3 shows the 1D modeling result and the resistivity variation before and after hydraulic fracturing. The relative variation is >30% at the frequencies <100 HZ. The results also show a maximum phase change of almost 20° at frequencies ~100 HZ. Figure 4 shows the 3D modeling results. If the slurry extent is 300 × 300 m, the surface observed apparent-resistivity variation is low (model-2). The simulation shows that additional injections up to nine times in volume (model-3 and model-4) yield greater variation. The results also indicate that surface AMT observations are more sensitive to the horizontal extent of the slurry than to its vertical thickness. That is, surface AMT is more sensitive to horizontal conductive plate-like fractures than to vertical fractures. This is an expected result because the direction of induced electric current flow is predominantly horizontal, and hence a horizontal conductive slab should generate stronger responses.

FIELD TEST

To evaluate the feasibility of using time-lapse AMT to monitor hydraulic fracturing, we have conducted a field test in southwest China. The fracture depth in the borehole at which the fracturing is performed is ~360 m. Several hydraulic fracturing tests have been made over the past several years. A second objective of the AMT monitoring is to delineate the boundaries of the injected slurry.

Geologic background

The geology in the test area consists primarily of the following major units: (1) black

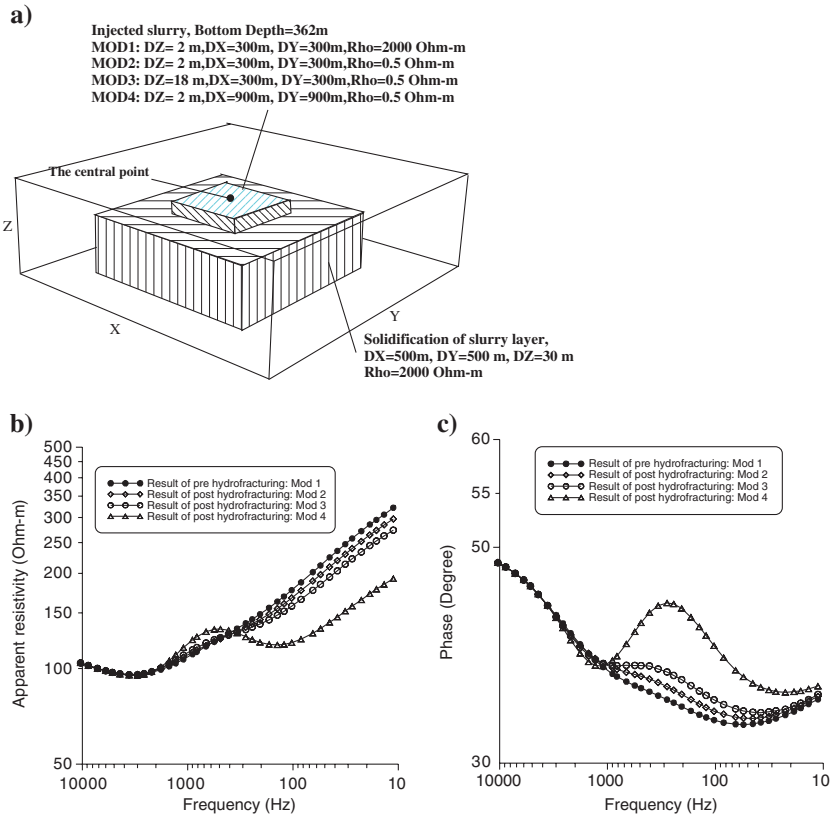

Figure 4. The 3D model and the modeling result. (a) Four models have calculated; the parameter of the model is illustrated in the sketch map of the 3D model. (b) The comparison of modeling apparent resistivity curve in the central point as shown in sketch map of the 3D model. (c) Three-dimensional modeling phase comparison result of the central point.

Ordovician laminar calcic sandstone and argillaceous limestone; (2) Silurian green limestone, argillaceous shale, and silty mudstone; (3) Devonian fine-grained quartzose sandstone, siltstone, and dolomite limestone; (4) Carboniferous ivory dolomite limestone and wine arenaceous shale and (5) Quaternary pebbles, fractured sandstone, gravel, and clay. The major stratum in the area is the top three segments ($S1_{1-3}$) Silurian Longmaxi Series. According to well log data, the lithology of the strata consist of argillaceous shales and argillaceous aleurolites. Core sample measurements indicate that the host rock has moderate resistivity values of ~100 ohm-m.

Data acquisition and processing

We performed 34 AMT soundings along four survey lines in the test area (Figure 5). Additionally, we laid out one site that was used as a remote reference that is located 6 km from the test area. Each site was occupied twice, once before hydraulic fracturing and once afterward. The time interval between the two observations is 3–6 days, and each survey was completed within three days (time span from the first to the last of the measurements at the 34 sites). Four sets of the MTU-5A instrumentation (Canada Phoenix Geophysics, with frequencies 12.5 Hz–12.5 kHz) were used for the data acquisition.

The recorded orthogonal components of the electromagnetic field were processed to determine the tensor impedance. Two pairs of nonpolarizing electrodes with a separation of 8–20 m were used to measure the electric field components, and two high-sensitivity magnetic coils were used to measure the horizontal magnetic field components. The time-domain measurements of the electric and

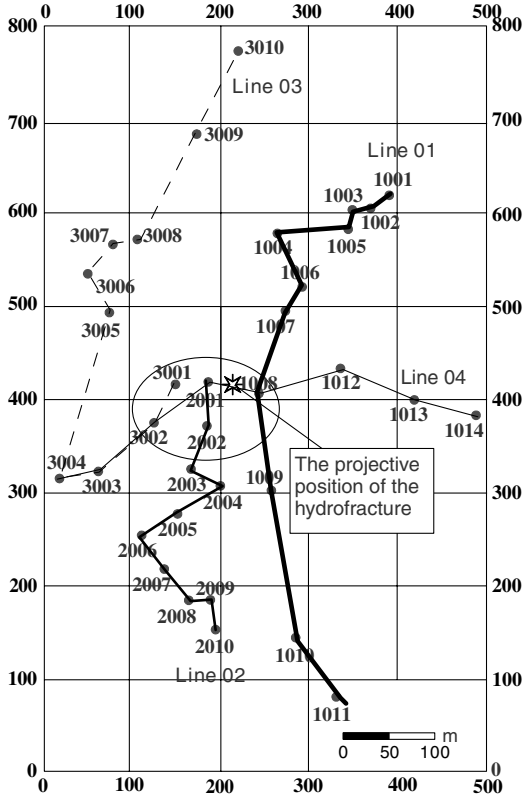

Figure 5. Field layout and location of the AMT station.

magnetic fields were converted to the frequency domain by Fourier transformation. The magnetotelluric amplitude and phase were calculated by estimating the transfer function from the converted measurements in the frequency domain. A calibration procedure was adopted to remove the instrument response. The horizontal electric fields (Ex, Ey) and the horizontal magnetic (Hx, Hy) field were transformed into the 2×2 magnetotelluric impedance tensor Z by using the V5-ROBUST MT and AMT data processing programs (version 3.0, http://www.phoenix-geophysics.com/Support/userguides). Most of the sounding sites contained high-quality data because there was little high-frequency noise in the area. Static shift correction has been applied for some stations using curve-shifting method (Beamish and Travassos, 1992) as shown in Figure 6b and 6e.

Analysis and discussion

The data analysis is based on detecting the difference in the apparent resistivities measured before and after hydraulic fracturing. According to the modeling results, there should be measurable differences in the raw field resistivity curves, so we analyzed these data first. Among the data from the 34 sites, there were significant changes (>200%) at six sites (1005, 1006, 3001, 3002, 2001, 2002), moderate changes (50 ~ 200%) at five sites (1007, 1008, 2003, 2004, 1009), and little or no change (< 50%) at the remaining sites. The locations of these sites are shown in Figure 5.

Figure 7a–7c shows the AMT apparent resistivity and its time variation at frequency 32.5 Hz: (a) is the apparent resistivity contour map before the hydraulic fracturing (b) is after the hydraulic fracturing, and (c) shows the relative change. There are two resistive anomalies prior to the fracturing (Figure 7a). One is centered on station 1006 and the other is centered on station 3001. The resistive zone around site 1006 might reflect the solidification of the injected slurry during a previous stage. The resistive body around site 3001 might reflect the solidification of the injected slurry in the current stage, because the fracture crack in the borehole is aligned southwest, and it is reasonable that the area of major solidification stays around site 3001. Figure 6b shows the apparent resistivity after the hydraulic fracturing survey. The apparent resistivity is lower overall than it was from the prehydraulic fracturing survey. Figure 7c is the contour map of the apparent resistivity change between pre- and posthydraulic fracturing surveys. The relative change $\delta = 0$ if there is no change in resistivity; if $\delta > 0$, the resistivity has increased after hydraulic fracturing. A change $\delta < 0$ is interpreted to be a change due to the fracturing and the presence of injected slurry.

Two areas in Figure 7c exhibit great apparent resistivity changes (>100%), one is near sites 1005 to 1006, and the other is near sites 3001 and 2002. Figure 7d–7f shows the result at frequency 22.5 Hz. Similar features are observed as at 32.5 Hz, except that the apparent resistivity change is greater near sites 3001 and 2001. Figure 7h and 7i shows the changes at 168.7 and 65 Hz; although there are some variations at 65 Hz, only minor variation occurs at 168.7 Hz. Given the maximum time lapsed between the surveys is only six days, and the area is close to the fracture center as shown in Figure 5, one explanation for the cause of the change is the injected presence of the slurry and the damage it caused to the host rock. It is difficult to judge whether the changes near site 1005 and 1006 are caused

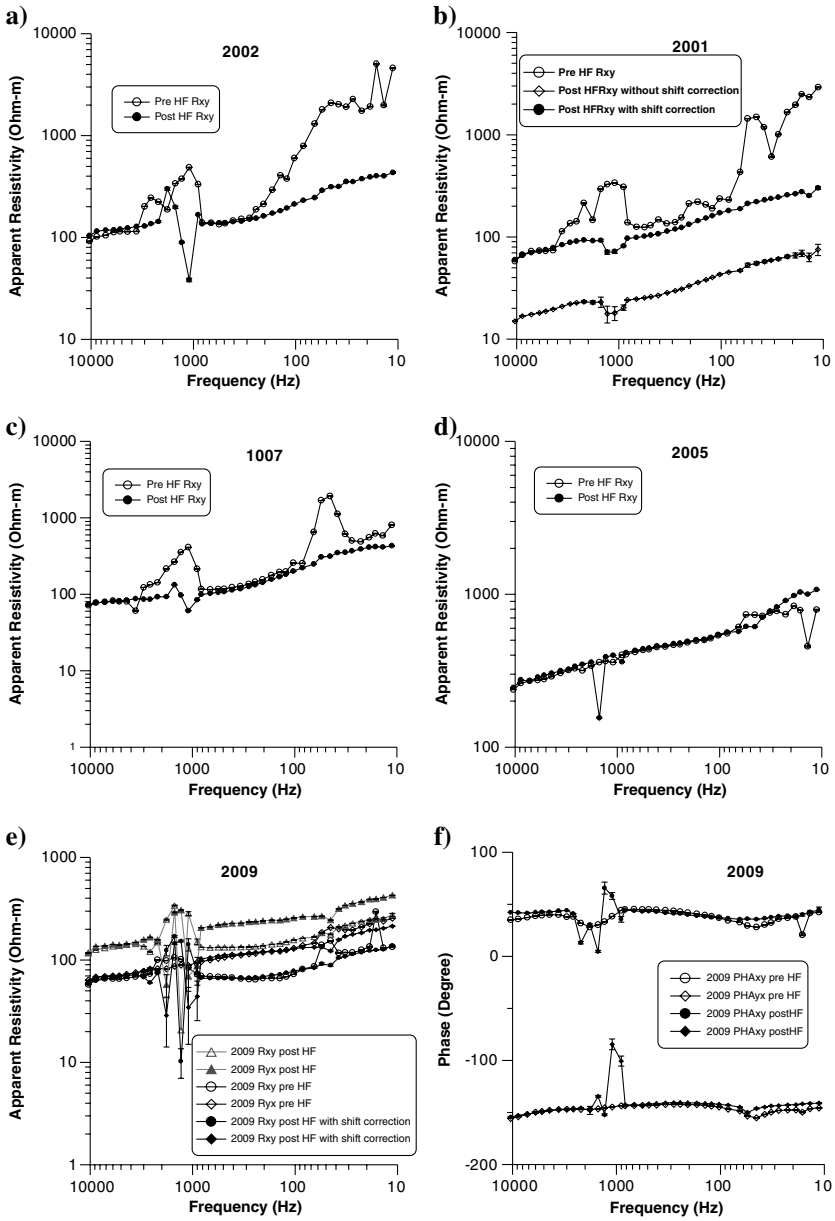

Figure 6. Example site to show the observed time-lapse AMT result; (a and b) show much apparent resistivity change, (c, d, and e) show far less change, (f) shows the phase change of site 2009. Shift correction is illustrated in (b and e); (e) also shows the variation of the other direction Ryx.

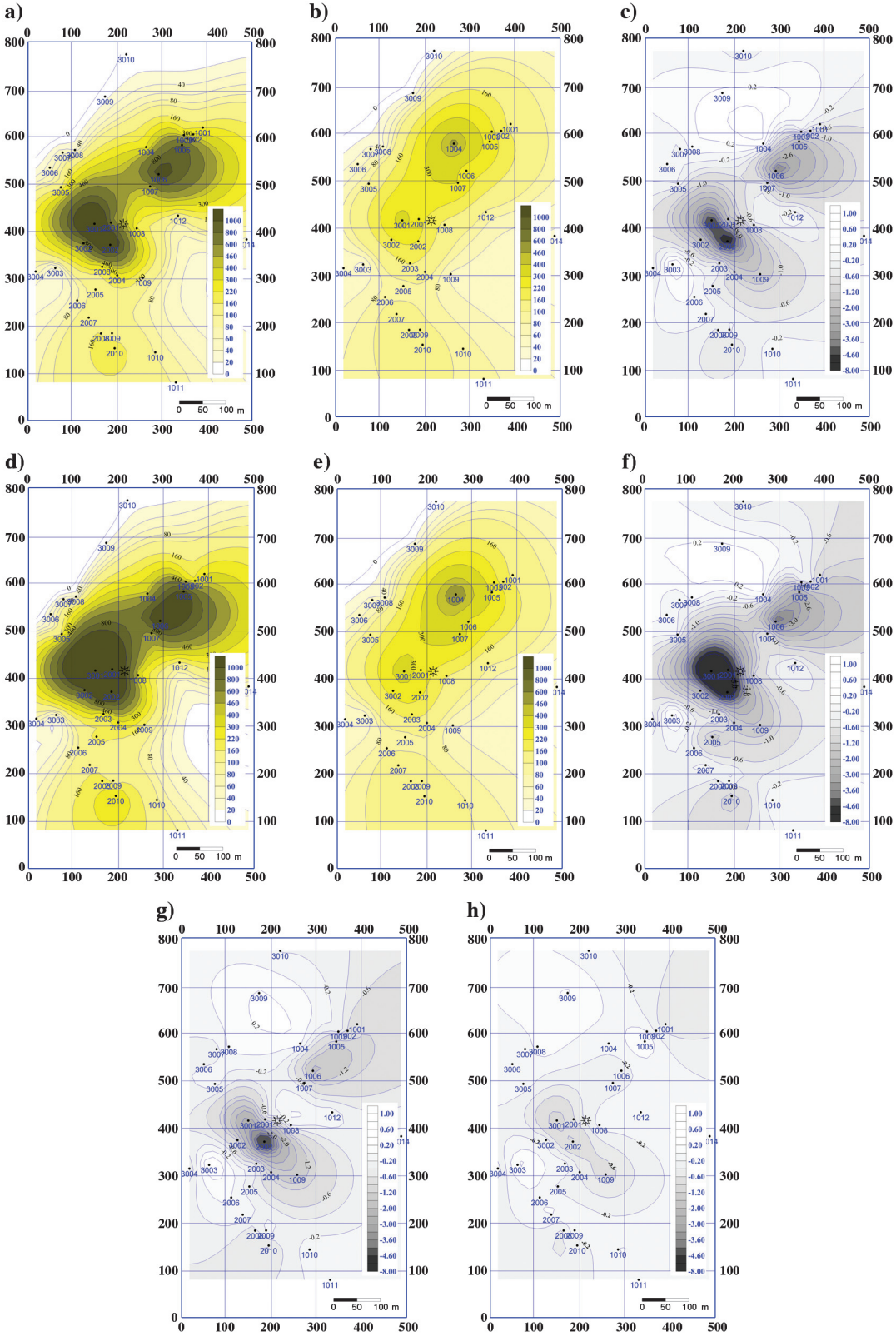

Figure 7. AMT mapping result of the test working area. (a) The prehydraulic fracturing apparent resistivity contour map at frequency 32.5 Hz; (b) is the posthydraulic fracturing apparent resistivity contour map; (c) is the variation ($\delta = 1 - \frac{\rho_{\text{pre}}}{\rho_{\text{post}}}$) imaging pre- and posthydraulic fracturing; (d-f) show a corresponding result of 22.5 Hz; (g and h) show a variation of 65 and 168.7 Hz

entirely by the fracturing, but there seems to be a strong correlation with the hydraulic fracturing. The nearby sites 1002 to 1004 do not show significant changes, so the noise interference can be excluded as an explanation. Therefore, we conclude that our field test has detected significant resistivity changes well above the level of natural variations after the hydraulic fracturing.

CONCLUSIONS

We have carried out a feasibility study on using AMT to monitor hydraulic fracturing based on laboratory sample measurements, numerical simulations, and a field test with a large number of survey stations. The laboratory resistivity measurements show that the injected slurry has a low resistivity increasing to a much higher resistivity after solidification. Time-lapse AMT apparent resistivities under natural conditions exhibit a normal resistivity change of <6%. Meanwhile, 1D and 3D numerical modeling based on the laboratory resistivity measurements and realistic geoelectric models yield changes before and after hydraulic fracture as large as 30%. Based on these findings, we surmise that time-lapse AMT could be used for monitoring and characterizing hydraulic fracturing. We have conducted a field test in which AMT data were acquired at 34 stations before and after a hydraulic fracturing event. The data show that AMT can delineate the boundary of previous injections of slurry, which are characterized by a high resistivity. Furthermore, the time-lapse data clearly exhibit significant decreases in the measured apparent resistivities after the injection of conductive slurry during the fracturing process. Thus, we conclude that time-lapse AMT could be a new means to monitor and map hydraulic fractures.

ACKNOWLEDGMENTS

Great thanks to the Associate Editor Mark Everett, reviewers Max Meju and Martyn Unsworth, and an anonymous reviewer for their insightful comments, which have greatly improved the manuscript. Great thanks also to Hu Zuzhi for providing the program of 3D modeling.

REFERENCES

Arthur, J. D., B. Bohm, and M. Layn, 2008, Hydraulic fracturing considerations for natural gas wells of the Marcellus shale: Presented at the Ground Water Protection Council 2008 Annual Forum, http://www.thefriendsvillegroup.com/HydraulicFracturingReport1.2008.pdf, accessed 12, April, 2012.

Beamish, D., and J. M. Travassos, 1992, A study of static shift removal from magnetotelluric data: Journal of applied geophysics, **29**, 157–178, doi: 10.1016/0926-9851(92)90006-7.

Chalikakis, K., V. Plagnes, and R. Guerin, 2011, Contribution of geophysical methods to karst-system exploration: An overview: Hydrogeology Journal **19**, 1–12.

Chiang, C. W., M. J. Unsworth, and C. C. Chien, 2008, Fault zone resistivity structure and monitoring at the Taiwan Chelungpu Drilling Project (TCDP): Terrestrial, Atmospheric, and Oceanic Sciences, **19**, 473–479.

Cuevas, N. H., J. W. Rector, and J. R. Moore, 2009, Electrokinetic coupling in hydraulic fracture propagation: 79th Annual International Meeting, SEG, Expanded Abstracts 1721–1725.

Eisel, M., and G. D. Egbert, 2001, On the stability of magnetotelluric transfer function estimates and the reliability of their variances: Geophysical Journal International, **144**, 65–82, doi: 10.1046/j.1365-246x.2001.00292.x.

Falgas, E., J. Ledo, A. Marcuello, and P. Queralt, 2006, Aquifer intrusion monitoring applying control source: Geophysical Research Abstracts, **8**, 07773.

Frid, V., A. Rabinovitch, and D. Bahat, 2003, Fracture induced electromagnetic radiation: Journal of Physics D: Applied Physics, **36**, 1620–1628, doi: 10.1088/0022-3727/36/13/330.

Frid, V., and K. Vozoff, 2005, Electromagnetic radiation induced by mining rock failure: International Journal of Coal Geology, **64**, 57–65, doi: 10.1016/j.coal.2005.03.005.

Garcia, X., and A. G. Jones, 2005, A new methodology for the acquisition and processing of audio-magnetotelluric (AMT) data in the AMT dead band: Geophysics, **70**, no. 5, G119–G126, doi: 10.1190/1.2073889.

Hanekop, O., and F. Simpson, 2006, Error propagation in electromagnetic transfer functions: What role for the magnetotelluric method in detecting earthquake precursors?: Geophysical Journal International, **165**, 763–774, doi: 10.1111/gji.2006.165.issue-3.

Hunt, A., N. Gershenzon, and G. Bambakidis, 2007, Pre-seismic electromagnetic phenomena in the framework: Tectonophysics, **431**, 23–32, doi: 10.1016/j.tecto.2006.05.028.

Kent, P., and J. Lee, 2007, Unconventional gas reservoirs-tight gas, coal seams, and shales, http://www.npc.org/StudyTopic Papers /29-TTG-Unconventional-Gas.pdf, accessed 29 September 2011.

Lodha, G. S., 1974, Quantitative interpretation of airborne electromagnetic response for a spherical model: M.S. thesis, University of Toronto.

Mackie, R. L., T. R. Madden, and P. E. Wannamaker, 1993, Three-dimensional magnetotelluric modeling using difference equations-theory and comparisons to integral equation solutions: Geophysics, **58**, 215–226, doi: 10.1190/1.1443407.

Mackie, R. L., J. T. Smith, and T. R. Madden, 1994, Three-dimensional electromagnetic modeling using difference equations: The magnetotelluric example: Radio Science, **29**, (4), 923–935, doi: 10.1029/94RS00326.

Maxwell, S., 2011, What does microseismic tell us about hydraulic fractures?: CSPG CSEG CWLS Convention, 1–5.

Maxwell, S. C., J. Rutledge, and R. Jones, 2010, Petroleum reservoir characterization using downhole microseismic monitoring: Geophysics, **75**, no. 5, 75A129–75A137, doi: 10.1190/1.3477966.

Murtaza, Y., 2011, Self-potential anomalies induced by water injection into hydrocarbon reservoirs: Geophysics, **76**, no. 4, F283–F292, doi: 10.1190/1.3596010.

Nie, B. S., X. Q. He, and C. W. Zhu, 2009, Study on mechanical property and electro magnetic emission during the fracture process of combined coal-rock: Procedia Earth and Planetary Science, **1**, 281–287, doi: 10.1016/j.proeps.2009.09.045.

Nitsan, U., 1977, Electromagnetic emission accompanying fracture of quartz-bearing rocks: Geophysical Research Letters, **4**, 333–336, doi: 10.1029/GL004i008p00333.

Orange, A., K. Key, and S. Constable, 2009, The feasibility of reservoir monitoring using time-lapse marine CSEM: Geophysics, **74**, no. 2, F21–F29, doi: 10.1190/1.3059600.

Rajib, K. S., S. Srivastava, and B. B. Bhattacharya, 2010, Audiomagneto telluric studies to trace the hydrological system of thermal fluid flow of Bakreswar Hot Spring, Eastern India: A case history: Geophysics, **75**, no. 5, B187–B195, doi: 10.1190/1.3431532.

Saleh, B., and P. Antoine Blum, 2005, Monitoring of fracture propagation by quartz tiltmeters: Engineering Geology, **79**, 33–42, doi: 10.1016/j.enggeo.2004.10.009.

Sheard, S. N., T. J. Ritchie, and R. Karen, 2005, Mining, environmental, petroleum, and engineering industry application of electromagnetic techniques in geophysics: Surveys in Geophysics, **26**, 653–669, doi: 10.1007/s10712-005-1760-0.

Sinharay, R. K., S. Srivastava, and B. Bimalendu, 2010,Audiomagnetotelluric studies to trace the hydrological system of thermal fluid flow of Bakreswar Hot Spring, Eastern India: A case history: Geophysics, **75**, no. 5, B187–B195, doi: 10.1190/1.3431532.

Song, F. X., K. H. Sadi, and M. N. Sadi Kuleli, 2010, An improved method for hydro fracture — Induced microseismic event detection and phase picking: Geophysics, **75**, no 6, A47–A52, doi: 10.1190/1.3484716.

Stanchits, S., S. Mayr, and S. Shapiro, 2011, Fracturing of porous rock induced by fluid injection: Tectonophysics, **503**, 129–145, doi: 10.1016/j.tecto.2010.09.022.

Steven, G., O. Keefe, and V. David, 1995, A mechanism for the production of electromagnetic radiation during fracture of brittle materials: Physics of the Earth and Planetary Interiors, **89**, 127–135, doi: 10.1016/0031-9201(94)02994-M.

Stow, S. H., and C. S. Haase, 1986, Subsurface disposal of liquid low-level radioactive waste at Oak Ridge, Tennessee: http://www.osti.gov/energycitations/servlets/purl/5557794-9rvlE3/ 5557794.pdf, accessed 29 September 2011.

Wang, Z. L., and John A. Stodt, 1991, Mapping hydraulic fracture using a borehole-to-surface electrical resistivity method: Geoexploration, **28**, 349–369, doi: 10.1016/0016-7142(91)90041-A.

Warpinskil, N. R., P. T. Branagan, and B. P. Engler, 1997, Evaluation of a downhole tiltmeter array for monitoring hydraulic fractures:: International Journal of Rock Mechanics & Mining Sciences, **503**, 129–145.

Willis, E. M., R. D. Burns, and R. R. Lu, 2007, Fracture quality from integrating time-lapse VSP and microseismic data: The Leading Edge, **26**, 1998–1202, doi: 10.1190/1.2780791.

Wilt, M., and M. Morea, 2004, 3D waterflood monitoring at Lost Hills with crosshole EM:: The Leading Edge, **23**, 489–493, doi: 10.1190/1.1756840.

Wong, H. Y., and I. W. Farmer, 1973, Hydrofracture mechanisms in rock during pressure grouting: Rock Mechanics and Rock Engineering, **5**, 21–41, doi: 10.1007/BF01246755.